

for the drop slowing down. A detailed calculation of the velocity drop would require the knowledge of the viscoelastic properties of the liquid crystalline polymer, which are quite complex. Nevertheless, if we approximate the polymer by a viscous liquid of typical viscosity $\eta = 10^4$ Pa·s, we obtain (16) a velocity on the order of $5 \mu\text{m/s}$, in agreement with the experimental results.

We have performed tack and dewetting experiments on a smectic polymer liquid crystal around the lamellar-to-isotropic phase transition. Specific behaviors that reflect the complex structure of the system are exhibited. Through the side-chain ordering, the smectic structure brings hardness and nonwettability. In contrast, in the isotropic phase, the presence of the backbone, which connects the side chains together, allows for a strong dissipation that leads to both a tacky behavior and an ability to slow down the dynamics of wetting. On each side of the phase transition, a different aspect of the hybrid macromolecule becomes predominant and imprints its behavior onto the system. This effect

can be used to design versatile materials with highly flexible properties that vary with temperature. Moreover, the transition temperature can be tuned by changing the copolymer composition, which may be useful for different types of applications. Finally, the reversibility of the structural transitions and of the resulting properties with temperature is another interesting feature of the system.

References and Notes

1. I. Langmuir, *Trans. Faraday Soc.* **15** (no. 3), 62 (1920).
2. A. G. Pittman, *Fluoropolymers*, L. A. Wall, (Wiley, New York, 1972), vol. 25.
3. R. Maoz and J. Sagiv, *J. Colloid Interface Sci.* **100**, 465 (1984).
4. C. D. Bain, J. Evall, G. M. Whitesides, *J. Am. Chem. Soc.* **111**, 7155 (1989).
5. P. Mansky, Y. Liu, E. Huang, T. P. Russell, C. Hawker, *Science* **275**, 1458 (1997).
6. A. Zosel, *Colloid Polym. Sci.* **263**, 541 (1985).
7. R. Clarke, A. Larson, E. E. Schmidt, S. P. Bitler, *Adhesive Age* (September 1993), p. 39.
8. C. Creton and L. Leibler, *J. Polym. Sci. Polym. Phys.* **34**, 545 (1996).
9. B. H. Rottink, K. te Nijenhuis, R. Addink, W. J. Mijis, *Polym. Bull.* **31**, 221 (1993).

10. T. Yamaguchi, T. Asada, N. Koide, *Mol. Cryst. Liq. Cryst.* **214**, 1 (1992).
11. P. G. de Gennes, *Rev. Mod. Phys.* **57**, 827 (1985).
12. A. Carre, J. C. Gastel, M. E. R. Shanahan, *Nature* **379**, 432 (1996).
13. M. E. R. Shanahan and A. Carre, *Langmuir* **11**, 1396 (1995).
14. ———, *J. Adhesion* **57**, 179 (1996).
15. M. E. R. Shanahan, *J. Phys. D* **21**, 981 (1988).
16. D. Long, A. Ajdari, L. Leibler, *Langmuir* **12**, 21, 5221 (1996).
17. F. Brochard-Wyart, F. Rondelez, C. Redon, *C.R. Acad. Sci. Paris Ser. II*, **306**, 1143 (1988).
18. F. Brochard-Wyart, J. M. di Meglio, D. Quéré, *ibid.* **304**, 553 (1987).
19. C. Andrieu, C. Sykes, F. Brochard, *J. Adhesion* **58**, 15 (1996).
20. C. Redon, F. Brochard-Wyart, F. Rondelez, *Phys. Rev. Lett.* **66**, 6 (1991).
21. T. Kasemura, S. Takahashi, N. Nakane, T. Maegawa, *Polymer* **37**, 16, 3659 (1996).
22. H. S. Van Damme, A. H. Hogt, J. Feijen, *J. Colloid Interface Sci.* **114**, 1, 167 (1986).
23. We thank A. C. Aubert la Fayette for synthesis of the copolymers. We are indebted to S. Girault for the structural investigation, C. Gay for fruitful discussion, and M. Bourrel and P. Tordjeman for the use of their probe tack tester.

12 March 1999; accepted 29 June 1999

Chemical "Double Slits": Dynamical Interference of Photodissociation Pathways in Water

R. N. Dixon,^{1*} D. W. Hwang,² X. F. Yang,^{2†} S. Harich,² J. J. Lin,²
X. Yang²

Photodissociation of water at a wavelength of 121.6 nanometers has been investigated by using the H-atom Rydberg tagging technique. A striking even-odd intensity oscillation was observed in the OH(X) product rotational distribution. Model calculations attribute this oscillation to an unusual dynamical interference brought about by two dissociation pathways that pass through dissimilar conical intersections of potential energy surfaces, but result in the same products. The interference pattern and the OH product rotational distribution are sensitive to the positions and energies of the conical intersections, one with the atoms collinear as H–OH and the other as H–HO. An accurate simulation of the observations would provide a detailed test of global H₂O potential energy surfaces for the three ($\tilde{X}/\tilde{A}/\tilde{B}$) contributing states. The interference observed from the two conical intersection pathways provides a chemical analog of Young's well-known double-slit experiment.

The photodissociation of water, a unimolecular process, can be studied from first principles, and extensive experimental and theoretical studies have been performed on

¹School of Chemistry, University of Bristol, Bristol BS8 1TS, UK. ²Institute of Atomic and Molecular Sciences, Academia Sinica, Taipei, Taiwan 106, R.O.C.

*To whom correspondence should be addressed. E-mail: r.n.dixon@bristol.ac.uk

†Permanent address: Laboratory of Plasma Physical Chemistry, Dalian University of Technology, Dalian 116024, China.

this system during the last few decades. Excitation in its longest wavelength ultraviolet absorption band between 150 and 200 nm populates the lowest excited (\tilde{A}) state. Dissociation from this state takes place on a single potential energy surface and forms an H atom and a ground-state OH ($X^2\Pi$) molecular product (1).

In contrast, three electronic states of the water molecule are implicated in its photochemistry at the Lyman- α wavelength ($\lambda = 121.6$ nm). The initial excitation is to the

third (\tilde{B}) state, which correlates adiabatically with an H atom and an excited electronic state of the OH partner ($A^2\Sigma^+$). However, the dominant dissociation leads to an H atom plus a ground-state OH molecule, which is brought about by a nonadiabatic crossing from the \tilde{B} state to the potential energy surfaces of either the \tilde{A} state or the ground (\tilde{X}) state of water. Although extensive information on the photodissociation through the \tilde{B} state has been obtained through these studies, a quantitative picture is still lacking.

Conical intersections of potential energy surfaces play an important role in the dynamics of many excited electronic states. The extremely high rotational excitation of the OH product that arises from excitation to the \tilde{B} state has been attributed to such an intersection. Dynamical calculations have shown that this high average rotational angular momentum results from a high torque acting in the vicinity of a conical intersection at a linear (H–O–H) geometry of the excited and ground-state potential energy surfaces of H₂O (2). This conical intersection arises because, for a linear approach of H to OH, a repulsive potential curve from H + OH($X^2\Pi$) can cross an attractive potential curve from H + OH($A^2\Sigma^+$), whereas there is an avoided crossing of these curves in the lower symmetry of a bent geometry.

Besides the conical intersection for the H–O–H geometry, there is second symmetry-determined conical intersection on the \tilde{B} state surface for the linear O–H–H geometry. The importance of this second intersection in the O(¹D, ³P) + H₂ reaction system has been

REPORTS

noted before (3, 4), but its possible influence on the photodissociation of H₂O has never been seriously addressed. Dixon and co-workers pointed out (5), in a recent wavepacket calculation, that a small part of the dissociative flux on the \tilde{B} state goes toward the second (O-H-H) conical intersection. That study indicated that this conical intersection might also play a role in the \tilde{B} state photodissociation.

We have now remeasured the H atom photofragment translational spectra from H₂O photodissociation at 121 nm at higher resolution by using a lower molecular beam temperature. A striking novel feature of the energy disposal, revealed by the data reported below, is an odd-even intensity alternation as a function of N , the OH rotational quantum number, superimposed upon the broad intensity distribution. This intensity alternation is due to interference between dissociation pathways via the two dissimilar conical intersections. The pattern of the intensity alternation is very sensitive to the positions of the two intersections, thus providing us a new probe to the H₂O potential energy surfaces.

Photodissociation of H₂O was investigat-

ed by using H-atom Rydberg "tagging," a time-of-flight (TOF) technique pioneered by Welge *et al.* (6). The experimental method used here has been described in detail before (7, 8). The rotational temperature of H₂O is estimated to be about 10 K. From the TOF spectra, the translational energy distributions can be obtained with a laboratory to center-of-mass transformation. Figure 1 shows the translational energy distributions of the products from H₂O photodissociation at 121.6 nm using two different polarization schemes (parallel and perpendicular to the detection axis). A TOF spectrum of the H atom product at the magic angle polarization was also made to ensure that the intensity ratio of the TOF spectra obtained at parallel and perpendicular polarization is correct. From these measurements, the angular dependence of the translational energy distribution can be constructed. Figure 2 shows a three-dimensional (3D) plot of the product translational energy distributions at different angles relative to the photolysis laser (121.6 nm) polarization direction. Because the total energy must be conserved in the dissociation process

$$h\nu + E_{\text{int}}(\text{H}_2\text{O}) - D_0(\text{H-OH}) \\ = E_{\text{trans}}(\text{H} + \text{OH}) + E_{\text{int}}(\text{OH}) \quad (1)$$

the internal energy (E_{int}) distribution of the OH products can be determined from the H atom translational energy (E_{trans}) distribution; h is Planck's constant, and D_0 the dissociation energy. All of the sharp features in the TOF spectra can be assigned based on previous spectroscopic data on the OH molecule (9, 10). Most of the ground-state OH($X^2\Pi$) products have extremely high rotational excitation within the $v = 0$ vibrational level, although there are a few products with rotational levels as low as $N = 0$ for the $v = 0$ state. Vibrationally excited OH products as high as $v = 4$ within the ground state were also observed, but were far fewer.

The oscillatory behavior in the OH ($X^2\Pi v = 0$) product rotational distribution when the laser polarization is parallel to the detection axis (Fig. 1) is highly reproducible. The odd N levels of OH($X, v = 0$) are more populated than would be interpolated between the even N levels. The cause of this oscillation in the OH product rotational distribution is not immediately clear. The even-odd N oscillation observed using the parallel polarization detection scheme is far less evident for the perpendicular detection scheme. This difference indicates that the dissociation process of H₂O might have two dissociation pathways to the ground-state OH product with very different dynamical behaviors: one with a clear even-odd rotational oscillation and one without this oscillation. The total rotational state distribution, which can be calculated by using the two distributions obtained from the parallel and perpendicular detection schemes, is peaked at $N = 45$ of OH(X). The overall distribution is similar to the theoretical results calculated through the H-O-H conical intersection pathway (4), indicating that the main dissociation process of H₂O to the OH ground state is probably through this conical intersection.

The OH products in the Λ -doublet components, the A' and A'' states, are unequally distributed. Figure 3 shows the experimental and simulated line shapes of the OH($N = 45$) line in the translational spectrum. This comparison shows that the observed line is narrower than predicted for a uniform population of the four fine structure components, and probably reflects the predicted propensity for conservation of A' or A'' symmetry from H₂O parent to OH product (4, 11), which would lead to unequal population of the A' and A'' Λ -doublet components for each N -value.

A periodic oscillation of rotational intensities is not of itself a new phenomenon and has been seen in the photodissociation of H₂O following excitation to the \tilde{A}^1B_1 state by photons with a wavelength of about 200

Fig. 1. The total translational energy distributions of the photofragments (H and OH) from H₂O photodissociation at 121.6 nm. The blue trace was obtained with the H-atom flight path parallel to the photolysis laser polarization direction; the red trace was obtained with detection perpendicular to the polarization direction. All sharp structures can be assigned to the rovibrational states of the OH($X^2\Pi, A^2\Sigma^+$) product. The assigned features correspond to the highly rotationally excited OH($X^2\Pi, v = 0$) product.

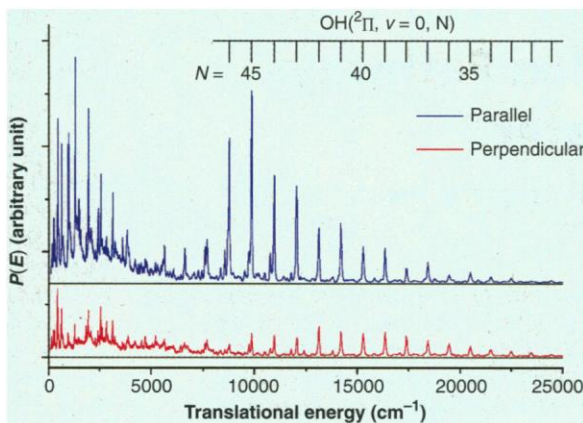
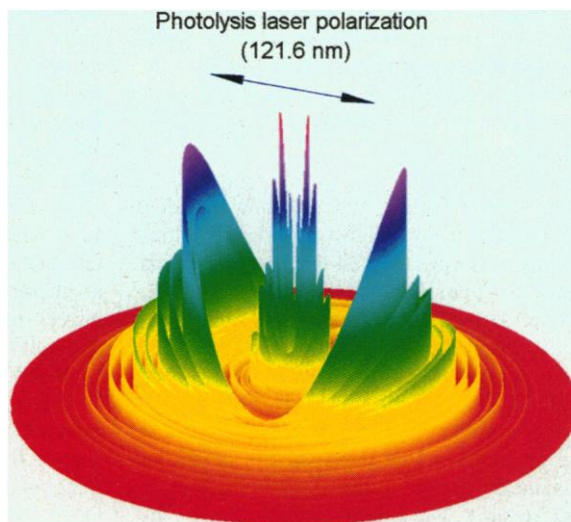


Fig. 2. The angular-dependent product translational energy distributions, relative to the polarization direction. The range of total translational energy shown is 0 to 25,000 cm⁻¹. Each sharp ring corresponds to fragmentation to a different quantum state of OH. The inner group of peaks relates to levels of the excited $A^2\Sigma^+$ state of OH, and the outer group to its ground $X^2\Pi$ state. Most of the highly rotationally excited OH products dissociate along the photolysis laser polarization direction.



REPORTS

nm, provided that the promotion is from a single ground-state vibration-rotation level. However, that is a perfect example of so-called Franck-Condon mapping of the initial bending motion of a parent molecule that dissociates under the influence of negligible torque (12). Schinke *et al.* have shown that this mapping leads to a sinusoidal modulation of the smooth rotational distribution with a period $\Delta N = \pi/\gamma_e$, where γ_e is the equilibrium angle (or $\pi-\gamma_e$, whichever is the smaller) (13). The observed period of about $\Delta N = 2.4$ for this \tilde{A}^1B_1 dissociation process corresponds to the known angle of $\gamma_e \approx 105^\circ$. But this model is clearly inappropriate for a process known to involve high torque and would also predict no oscillation for dissociation from a linear H-OH geometry.

Many ab initio calculations have confirmed the existence of the conical intersection in each of the two equivalent H + OH and HO + H exit channels for linear HOH. However, there can be no interference between motion along these two channels because they lead to physically distinct products. Indeed, we have observed an intensity alternation for the process $\text{HOD} + h\nu \rightarrow \text{D} + \text{OH}$ similar to that for H_2O . We therefore seek an alternative explanation.

The earlier dynamical calculation by one of us using time-dependent wavepackets, which was able to reproduce the general form of the OH population distribution, showed no evidence of any intensity alternation (11). That calculation was based on the ab initio surfaces of Theodorakopoulos *et al.* (14). These surfaces did not cover the full range of angles and distances and had to be semi-empirically extended before use. Although it was known from symmetry arguments that there must be a second conical intersection for linear geometries of the type H-H-O, these were thought to occur at very high energy and therefore to be of no importance. However, Yarkony has more recently calculated limited regions of the surfaces in the vicinity of these two types of crossing (15), and it is now clear that

both are energetically accessible for excitation of water at 121.6 nm. We now consider the possibility of interference between the exit channels H+OH and H+HO.

There are several important quantum numbers for the dissociation process: J , K_a , and K_c for the rotation of the parent H_2O molecule, and λ (the helicity) for its component along the direction of the departing H atom; N for the rotation of the OH molecule (neglecting electron spin for the moment), Λ ($= 1$) for its orbital angular momentum, and a designation A' or A'' for its Λ -doublets (which reflect the orientation of the unpaired electron orbital with respect to the OH plane of rotation). At large H-OH distance, where the OH rotation becomes free, the number of angular nodes in its rotational wavefunction increases with its quantum number N . Consequently the mapping of the outgoing wavefunction for a $^1A'$ parent surface onto the OH rotational wavefunctions has a symmetry property (denoted by m) with respect to H + OH ($\theta = 0$) and H + HO ($\theta = \pi$) at the same intersystem distance R , where θ is the angle between the OH bond and \mathbf{R} (Table 1).

Thus, for each H+OH exit channel, a coherent passage of the outgoing wavefunction from the \tilde{B}^1A_1 surface onto the \tilde{X}^1A_1 surface through both conical intersections may result in a constructive or destructive interference of the waves, depending on their relative amplitudes and phases, and the symmetry number m . Conversely, for dissociation through electronic Coriolis (Renner-Teller) coupling to the $\tilde{A}^1B_1(^1A'')$ surface, all of the symmetries in Table 1 should be reversed. This latter coupling is zero for $\lambda = 0$, and increases in strength with increasing λ (16).

We first consider a simple model for the two $^1A'$ pathways in which one such component wave exits near $\theta = 0$ at an intersystem distance R_0 with amplitude A_0 and the second exits near $\theta = \pi$ at distance R_π with amplitude A_π . For a given rotational state N_i of the OH product, the final outgoing free waves will have a wave-vector k_i that will be a function of the available

energy following dissociation and will be the same for both pathways:

$$\frac{k_i^2 \hbar^2}{2\mu} = E_{\text{avail}} - E_{\text{OH}}(N_i) \quad (2)$$

where $\hbar = h/2\pi$ and μ is the reduced mass of H-OH. The expression for the product population will therefore contain the N -dependent factor:

$$|A_0 + mA_\pi \exp(i k_i (R_\pi - R_0))|^2 \quad (3)$$

If $(R_\pi - R_0)$ is small, the presence of m in this expression will lead to an alternation of population over a sustained range of N -values for the A' series of OH rotational levels. A similar interference may occur for the A'' levels, although in this case the crossings to the $^1A''$ surface can take place over the wider range of R -values for which the potential functions for the \tilde{B} and \tilde{A} states are degenerate. For each value of N , the A' and A'' levels are close in energy (Fig. 3). If these levels are unresolved, and in the eventuality that the amplitudes A_0 and A_π contribute equally to both series, then this alternation would be hidden by their opposite phase behavior. Fur-

Fig. 3. Experimental evidence for the Λ -doublet propensity in the OH photofragment. In the simulation, all four fine-structure components of $\text{OH}(X^2\Pi, v=0, N=45)$ are assumed to be equally populated. The width of each individual component is assumed to be 45 cm^{-1} , corresponding to a translational energy resolution of 0.45%. The obvious disagreement between the experimental and simulated line-width clearly indicates that this assumption is incorrect: most probably, the Λ -doublet components are unevenly populated.

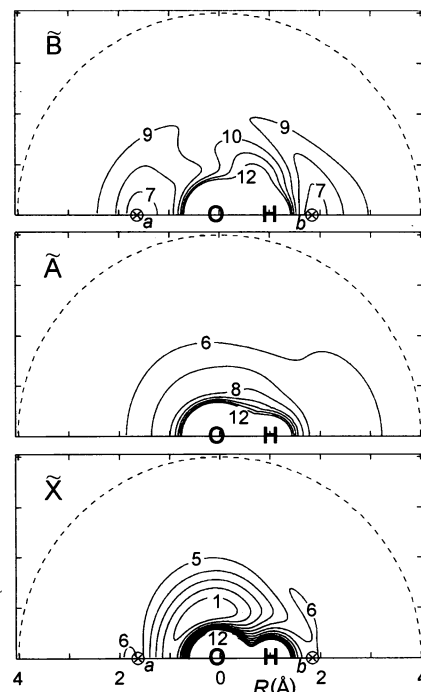
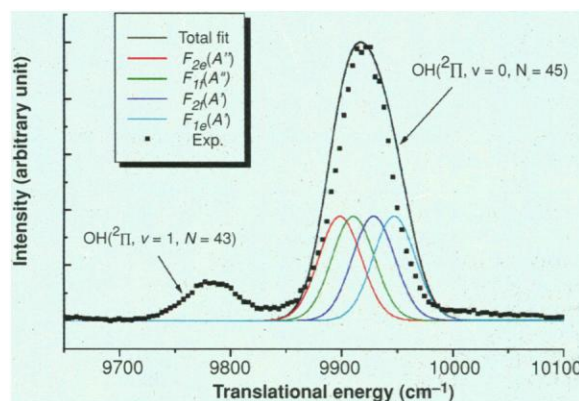


Fig. 4. Contours of the \tilde{B} -, \tilde{A} -, and \tilde{X} -state potential energy surfaces for the movement of H around OH with a fixed OH bond length of 1.07 Å. Energies are given in electron volts relative to the minimum of the ground state. The conical minima (\otimes), a (H-OH) and b (H-HO), of the \tilde{B} -state potential are degenerate with the conical maxima, a and b, of the \tilde{X} -state potential, leading to the "funneling" of nuclear trajectories from \tilde{B} to \tilde{X} . The \tilde{B} surface is asymptotic to $\text{H} + \text{OH}(A^2\Sigma^+)$ at large H-OH separation, whereas the \tilde{A} and \tilde{X} surfaces are asymptotic to $\text{H} + \text{OH}(X^2\Pi)$. The central core of each potential function is strongly repulsive.

REPORTS

thermore, should $(R_\pi - R_0)$ be large, or the varying OH energy be accompanied by a strong variation of k_i with N , then any such interference will only be sustained over a short range of N -values. Thus, the pattern of any observed interference is a sensitive probe of the overall dynamics.

These ideas have been tested by new dynamical calculations. An accurate theoretical treatment of the process would require complete 3D surfaces for the three important electronic states, together with the non-adiabatic couplings between these, to be used in 3D dynamical calculations that include a range of parent rotational states. For the present we restrict ourselves to a model calculation that demonstrates the basic principles. Murrell and co-workers have published analytical expressions for 3D surfaces for the two 1A_1 states (17), and for the \tilde{A}^1B_1 state (18). The latter surface was not completely degenerate in linear geometries with that for the \tilde{B} state, as required by their common $^1\Pi$ character, and small shifts were made to remedy this defect. These surfaces (Fig. 4) are based on

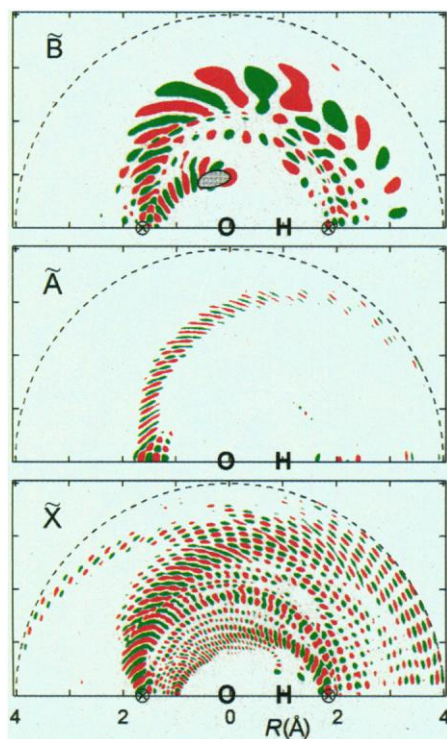


Fig. 5. The outgoing waves on the three H_2O surfaces, resonant at an energy appropriate to excitation to the \tilde{B} state at the Lyman- α wavelength, with $J' = 1$ and $\lambda = 1$. Green and red lobes have positive and negative amplitudes, respectively, and have been truncated beyond $R = 4 \text{ \AA}$. The gray-filled contour on the \tilde{B} surface represents the Franck-Condon excitation from the ground state. Note the strong interference between waves emanating from the two conical intersections (\otimes) on the ground-state (\tilde{X}) surface, but not on the \tilde{A} surface.

a combination of experimental and ab initio data, and possess all of the expected topological features (19). However, it must be stressed that they are not energetically accurate in all aspects.

For simplicity, the dynamical calculations were limited to two active dimensions, with one r_{OH} fixed at 1.07 \AA reflecting the mean bond length for the centrifugally stretched OH product with high N -values. Thus, only one bond could break after passing through either of the linear H-OH or H-HO intersections. The spin doubling of the OH levels was neglected, because at high rotation of OH its electron spin becomes decoupled from its internuclear axis, and will therefore be a spectator to the nuclear dynamics. Figure 5 presents the outgoing waves on the three surfaces resonant at an energy appropriate to excitation to the \tilde{B} state at the Lyman- α wavelength. For this calculation, $J' = 1$ and $\lambda = 1$, being the dominant term in excitation through a type- b transition from the lowest (0_{00}) level of the H_2O ground state. These plots are polar presentations of $\chi(R, \theta)$ for the motion of the departing H atom from the OH moiety and have been truncated for clarity at $R = 4 \text{ \AA}$ (the semicircles). Because the polar angle θ is restricted to the range $(0 - \pi)$, passage through linearity is represented by reflection at the diagonal of the semicircles.

The wave on the \tilde{B} surface is initiated in the Franck-Condon region (open contour) and is accelerated towards the linear H-OH intersection point (a in Fig. 4). The flux then becomes partitioned into three components. The major component is transmitted onto the \tilde{X} surface, on which it proceeds outwards leading to dissociation to $H +$

OH(X). (Note that in a space fixed frame, this motion would be shared between the departing H atom and the rotation of its OH partner.) A minor component is transmitted through Renner-Teller coupling onto the \tilde{A} surface and also dissociates to $H + OH(X)$. However, a significant flux remains on the \tilde{B} surface and the H- and OH-moieties continue their relative orbiting motion. Part of the flux dissociates on the \tilde{B} surface, leading to $H + OH(A)$, but part is attracted towards the linear H-HO intersection, (point b), which provides a second source of flux on the \tilde{X} surface (and in principle on the \tilde{A} surface). The interference between these two sources of flux on the \tilde{X} surface is indicated by the pattern of nodes in the wave-function as the two components spiral out in opposite directions.

The population distribution over the two sets of Λ -doublets of the OH X-state calculated with the wave-functions on the \tilde{A} and \tilde{X} surfaces is given in Fig. 6. (Experiments show that there is substantial vibrational excitation for the OH A-state (20) that is not accessible with the frozen bond length of the present calculation.) The distribution over the A' Λ -doublets shows a sustained intensity alternation, with even N stronger from $N = 22$ to 36. The phase then reverses, and from $N = 39$ to 43 the population is higher for odd N . In contrast, the population distribution for the A'' Λ -doublets is much smoother and peaks at a lower N -value than for the A' Λ -doublets. Interference occurs between two emanating waves for the A' case; but not for the A'' case for which the nonadiabatic transition from \tilde{B} to \tilde{A} takes place almost entirely through H-OH geometries (Fig. 5).

These distributions should be contrasted with the smooth distributions of (11), calculated with the same computer program but with the potentials from (14). Even so, there are still several quantitative differences between the results of Fig. 6 and the experimental data of Fig. 2. In particular the calculated oscillation depth is too high, and its phase is incorrect. In part, these shortcomings can be attributed to errors in the chosen potential functions. The minimum energies and locations of the two conical intersections for these functions are given for the calculations of Murrell *et al.*

Table 1. Values of the symmetry index m for the ratios at $\theta = 0$ and $\theta = \pi$ of the mapping of the bending motion of H_2O in $^1A'$ states onto OH rotational states. The signs of m are reversed for the mapping from $^1A''$ states.

| Quantum numbers ($N - \Lambda + \lambda$) | Λ -doublets | m |
|--|---------------------|-----|
| Even | A' | +1 |
| Odd | A' | -1 |
| Even | A'' | -1 |
| Odd | A'' | +1 |

Table 2. Calculated locations and minimum energies of the two conical intersections of the \tilde{B} and \tilde{X} potential functions of H_2O .

| Calculation | R | $V(R, \theta) - E(H + OH, X)$ |
|--------------------------------|-------------------|-------------------------------|
| Murrell <i>et al.</i> (17, 18) | | |
| H-OH ($\theta = 0$) | 1.71 \AA | 0.61 eV |
| H-HO ($\theta = \pi$) | 1.81 \AA | 0.65 eV |
| Yarkony (15) | | |
| H-OH ($\theta = 0$) | 1.70 \AA | 0.71 eV |
| H-HO ($\theta = \pi$) | 1.83 \AA | 1.46 eV |

in Table 2. The later, more accurate, treatment by Yarkony of the conical intersections (15) notes that in three dimensions, there are seams of crossings as a function of the two bond-lengths, which have absolute minima with Yarkony's parameters in Table 2.

With this latter potential, the much greater difference in potential between V_0 and V_π would affect the outgoing wave in two ways. (i) The forces of attraction toward the second intersection would be weakened, lowering the ratio of A_π to A_0 (see eq. 3) and thus decreasing the depth of the interference. (ii) Secondly, the relative phases of A_π and A_0 , and thus the phase of the interference, would be affected by the accompanying change in the profile of the \tilde{B} -state potential between the two conical intersections. The model calculation has almost certainly overestimated the strength of the interference.

A second important factor is the purity of excitation, and particularly of the helicity quantum number λ which is directly related to the phase of the interference (Table 1). But λ is not a good quantum number. Even for excitation from the 0_{00} level of water the type-*b* moment of the \tilde{B} - \tilde{X} transition, which is directed along the bisector of the two bonds, makes an angle of about 56° to the recoil vector \mathbf{R} (H-OH). Thus the projection of \mathbf{J} onto \mathbf{R} corresponds to 70% of $\lambda = 1$ and 30% of $\lambda = 0$. Furthermore, even at our estimated beam temperature of 10 K, 76% of the ground-state molecules are in levels higher than 0_{00} (mainly 1_{01}), resulting in fragmentation from a number of levels with a range of values of λ . This effect will lead to a further dilution of the interference depth. We note in this respect that there was no hint of an intensity alternation in the spectra for this system presented in (5), for which the molecular beam

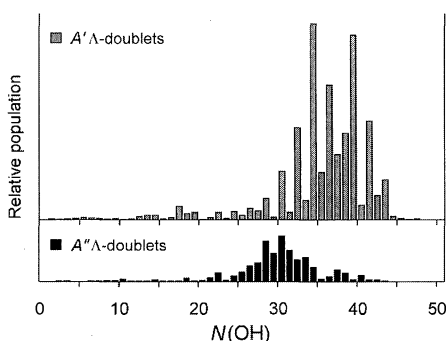


Fig. 6. The calculated population distribution for the Λ -doublet components of the OH ground state. The A' Λ -doublets will contribute to the time-of-flight spectrum most strongly in parallel polarization, and the A'' Λ -doublets in perpendicular polarization. The marked alternation for the A' components relates to the interference noted in Fig. 5.

temperature was ~ 100 K.

Thirdly, in the real molecule the nonadiabatic transition between the \tilde{B} and \tilde{X} states can take place over the ranges of values of R which correspond to the seams of intersection in the full three dimensions.

Finally, the results of Fig. 6 lead to an understanding of the observation that the intensity alternation is only present for parallel polarization. The anisotropy of fragmentation following the \tilde{B} to \tilde{X} crossing will be controlled by the same factors as operate for the \tilde{A} to \tilde{X} crossing at a conical intersection in NH_3 . The observations for ammonia have been rationalized using a classical, energy and angular momentum conserving impact parameter model. It is assumed that the final momenta are established at the "point" of the conical intersection, for which the atoms are coplanar (21). Applying this model to H_2O , by the time that the HOH angle has opened to reach an H-OH intersection, the line of atoms will be approximately perpendicular to the axis of the excitation transition moment, with both H atoms moving parallel to this axis. Thereafter, if the molecule makes a \tilde{B} to \tilde{X} transition, the nascent OH will rotate with high angular momentum while the free H atom will tend to continue in a straight line, particularly when in partnership with the highest N -states of OH, leading to a dominant parallel polarization. However, any subsequent \tilde{B} to \tilde{X} transition via the H-HO conical intersection will tend to degrade the anisotropy from this limiting behavior.

In contrast, the \tilde{B} to \tilde{A} transition involves an interchange between nuclear and electronic angular momentum, the effects of which have been successfully modeled for the predissociation of HCO (22). The consequence of this quantum phenomenon, for the case where $\lambda = 1$, is that after the transition the atoms tend to move in a plane which has become rotated by 90° about the linear axis, and thus perpendicular to the original excitation transition moment. Given that the \tilde{B} to \tilde{X} transition is subject to quantum interference, but the \tilde{B} to \tilde{A} transition is not (Fig. 6), it follows that the interference should be most clearly observed in parallel polarization, as observed.

References and Notes

- P. Andresen, G. S. Ondrey, B. Titze, *J. Chem. Phys.* **80**, 2548 (1984).
- K. Weide and R. Schinke, *ibid.* **87**, 4627 (1987).
- T.-S. Ho, T. Hollebeek, H. Rabitz, L. B. Harding, G. C. Schatz, *ibid.* **105**, 10472 (1996).
- G. C. Schatz, *ibid.* **83**, 5677 (1985).
- D. H. Mordaunt, M. N. R. Ashfold, R. N. Dixon, *ibid.* **100**, 7360 (1994).
- J. Biesner *et al.*, *ibid.* **91**, 2901 (1989), and references therein.
- L. Schnieder, K. Seekamp-Rahn, E. Wrede, K. H. Welge, *ibid.* **107**, 6175 (1997). The H(D) atom products from the photodissociation of H_2O (HOD or D_2O) in a

molecular beam are excited in the photolysis region to their $n = 2$ electronic state using the 121.6 nm vacuum ultraviolet (VUV) light, generated using the two photon-resonant ($2\nu_1 - \nu_2$) four-wave mixing scheme in a cell with Kr/Ar gas mixture (8). $2\nu_1$ (212.5 nm) is resonant with the Kr ($4p-5p$) transition. The ν_1 laser light is generated by doubling a dye laser pumped by the third harmonic (355 nm) of a Nd:YAG laser: ν_2 (845 nm) is the direct output of a dye laser pumped by the second harmonic of the same YAG laser. During the experiment, normally a few millijoules of 212.5 nm and 845 nm laser light were used. After VUV excitation, the H atom is sequentially excited to a higher Rydberg state with $n \sim 80$ using 365-nm light, generated by doubling a dye laser pumped by the same YAG laser. The neutral Rydberg H/D atom then flies about 38 cm to reach a multichannel plate (MCP) detector. The molecular beam is generated by expanding a mixture of H_2O in Ar through a pulsed nozzle with a pulse duration of about 100 μs . The mixture is made by bubbling Ar through the water sample at room temperature. By changing the Ar carrying pressure, different expansion conditions with different H_2O concentrations can be achieved. The spectra were taken at a total stagnation pressure of 600 torr of a 3% $\text{H}_2\text{O}/\text{Ar}$ mixture. The detection axis, the molecular beam, and the photolysis laser beam are all perpendicular to each other in this experiment. The VUV laser serves as both the photolysis laser and the laser for Lyman- α excitation. The polarization of the 121.6 nm laser light can be changed by rotating the polarization of the 845-nm laser using a rotatable half-waveplate.

- J. P. Marangos, N. Shen, H. Ma, M. H. R. Hutchinson, J. P. Connerade, *J. Opt. Soc. Am. B* **7**, 1254 (1990).
- G. H. Dieke and H. M. Crosswhite, *J. Quant. Spectrosc. Radiat. Transfer* **2**, 97 (1962).
- E. R. Comben and J. M. Brown, *Chem. Phys.* **119**, 443 (1988).
- R. N. Dixon, *J. Chem. Phys.* **102**, 301 (1995).
- R. Schinke, V. Engel, V. Staemmler, *ibid.* **83**, 4522 (1985). Classically, the smooth distribution of zero-point bending momentum at short H-OH distance becomes a smooth distribution of rotational motion of the OH(X) fragments at large H-OH distance. The equivalent quantum-mechanical model involves the mapping of the bending wave-function onto the product rotational wave-functions. But the latter are oscillatory functions of the angle between the OH bond and the recoil axis of the departing H-atom. Thus, the mapping of a bending wave-function which is restricted to a narrow range of angles can lead to an oscillation in the OH rotational population.
- R. Schinke, R. L. Vander Wal, J. L. Scott, F. F. Crim, *J. Chem. Phys.* **94**, 283 (1991).
- G. Theodorakopoulos, I. D. Petsalakis, R. J. Buenker, *Chem. Phys.* **96**, 217 (1985).
- D. R. Yarkony, *Mol. Phys.* **93**, 971 (1998).
- R. N. Dixon, *ibid.* **54**, 333 (1985).
- J. N. Murrell, S. Carter, S. C. Farantos, P. Huxley, A. J. C. Varandas, *Molecular Potential Energy Functions* (Wiley-Interscience, New York, 1984).
- H. Guo and J. N. Murrell, *J. Chem. Soc. Faraday Trans. 2* **84**, 949 (1988).
- The dynamical calculations were carried out using the diabatic representation of Murrell *et al.* (17), and then transformed to the adiabatic representation for Figs. 4 and 5. This simplifies the treatment of geometric phase effects around conical intersections.
- R. N. Dixon *et al.*, in preparation.
- D. H. Mordaunt, M. N. R. Ashfold, R. N. Dixon, *J. Chem. Phys.* **104**, 6460 (1996).
- S. H. Kable *et al.*, *J. Phys. Chem.* **95**, 8013 (1991).
- R.N.D. is grateful to the Leverhulme Trust for the award of an Emeritus Research Fellowship. The experimental work was done at IAMS, supported by the National Science Council and the Academia Sinica of the Republic of China. X.Y. wishes to thank Y. T. Lee and K. Liu for helpful discussions.

4 May 1999; accepted 9 July 1999